Contribution from the Chemistry Department,
The University of North Carolina, Chapel Hill, North Carolina 27514

Reactivity of the Oxo-Bridged Ion $[(bpy)_2(O)Ru^{IV}ORu^{V}(O)(bpy)_2]^{3+}$

Stephen J. Raven and Thomas J. Meyer*

Received February 17, 1988

The μ-oxo ion $[(bpy)_2(O)Ru^{IV}ORu^{V}(O)(bpy)_2]^{3+}$ (bpy = 2,2'-bipyridine) has been generated in solution by electrochemical or chemical oxidation of $[(bpy)_2(HO)Ru^{III}ORu^{IV}(OH)(bpy)_2]^{3+}$. The IV-V complex, which is a powerful oxidant, is reduced by water to give O_2 by a pH-independent reaction that is first order in oxidant; k(25 °C, μ = 0.1 M) = 3.0×10^{-4} s^{-1}. Both the IV-V complex and its pyridine analogue, $[(bpy)_2(py)Ru^{III}ORu^{V}(O)(bpy)_2]^{4+}$ (py = pyridine), are facile oxidants toward a variety of organic functional groups.

Introduction

The existence of higher oxidation states of ruthenium and osmium based on oxo formation has been well documented.[1-7] In the chemistry of ruthenium, a striking example is the μ-oxo dimer $[(bpy)_2(H_2O)Ru^{III}ORu^{III}(H_2O)(bpy)_2]^{4+}$ (bpy is 2,2'-bipyridine).[3b] Oxidation of this ion and some of its derivatives occurs by the loss of $4H^+$ and 4e to give $[(bpy)_2(O)Ru^{V}ORu^{V}(O)bpy)_2]^{4+}$, which, in turn, oxidizes water to dioxygen or chloride to Cl_2.[3b,4,8]

In addition to the III-III and V-V states, electrochemical studies show that there are pH-potential domains where the μ-oxo structure stays intact in oxidation states II-II, III-III, III-IV, and IV-V.[3b,5a] Because of the existence of strong μ-oxo-induced electronic coupling between the metal ions, the assignment of oxidation states in these complexes is only descriptive. For example, for the "III-IV" μ-oxo complex, a more appropriate description may be the delocalized description III.5-III.5. From electrochemical studies, the oxidation state IV-IV is thermodynamically unstable over the pH range 0-14. Below pH = 2.5 the IV-V state is unstable with respect to disproportionation via

$$3[(bpy)_2(O)Ru^{IV}ORu^{V}(O)(bpy)_2]^{3+} + 3H^+ \rightarrow 2[(bpy)_2(O)Ru^{V}ORu^{V}(O)(bpy)_2]^{4+} + [(bpy)_2(OH_2)Ru^{III}ORu^{IV}(OH)(bpy)_2]^{4+} \quad (1)$$

Given the remarkable reactivity characteristics of the μ-oxo ion in oxidation state V-V, the descriptive chemistry and the reactivity properties of oxidation state IV-V were of interest to us. In this oxidation state (1) the μ-oxo complex is a strong oxidizing agent

$$[(bpy)_2(O)Ru^{IV}ORu^{V}(O)(bpy)_2]^{3+} + 2H^+ + 2e^- \rightarrow [(bpy)_2(OH)Ru^{III}ORu^{IV}(OH)(bpy)_2]^{3+}$$

$$E^{\circ\prime} = 0.85 \text{ V vs SSCE at pH} = 7, \mu = 0.1 \text{ M}$$

(2) it has the capability of acting as a multiple-electron oxidant and from pH = 2.5-14 is thermodynamically capable of oxidizing water to dioxygen

$$2[(bpy)_2(O)Ru^{IV}ORu^{V}(O)(bpy)_2]^{3+} + H_2O \rightarrow 2[(bpy)_2(OH)Ru^{III}ORu^{IV}(OH)(bpy)_2]^{3+} + O_2$$

$$\Delta G^{\circ\prime} = -1.1 \text{ eV at pH } 7, \mu = 0.1 \text{ M}$$

and (3) given the background synthetic chemistry, the IV-V complex is one of a series of related μ-oxo oxidants, a related case being the μ-oxo ion $[(bpy)_2(py)Ru^{III}ORu^{III}(H_2O)(bpy)_2]^{4+}$, which undergoes two successive, one-electron oxidations to give $[(bpy)_2(py)Ru^{III}ORu^{IV}(OH)(bpy)_2]^{4+}$ and then $[(bpy)_2(py)Ru^{III}ORu^{V}(O)(bpy)_2]^{4+}$.[7]

We describe here the generation and solution properties of the IV-V complex and of its reactivity toward both water and a variety of organic substrates.

Experimental Section

Materials. The water used in analytical measurements was purified by a Millipure system. Because of the extreme reactivity of the oxidized μ-oxo complexes, it is essential that the water used be free of trace organics. Buffer solutions for electrochemical, kinetic, and spectroscopic measurements were prepared from mono-, di-, and tribasic phosphate (pH = 3-12) at a constant ionic strength of 0.1 M. The pH measurements were made by using a Radiometer pHM62 pH meter. NaOCl was purchased as an aqueous reagent (5%) from Alfa products and its concentration determined iodometrically, before use, by allowing it to react with an excess of iodide in acidic solution. The iodine produced was titrated with a standard sodium thiosulfate solution. All other materials were obtained as reagent grade and used without further purification.

Preparations. $[(bpy)_2(OH)RuORu(OH)(bpy)_2](ClO_4)_3$ and $[(bpy)_2(py)RuORu(OH)(bpy)_2](ClO_4)_4$ were prepared as described previously.[3b,7] All organic reagents were obtained from the Aldrich Chemical Co. and purified by vacuum distillation or recrystallization.

Solutions Containing $[(bpy)_2(O)Ru^{IV}ORu^{V}(O)(bpy)_2]^{3+}$. Procedure 1. A solution containing a known concentration of $[(bpy)_2(OH)RuORu(OH)(bpy)_2](ClO_4)_3$ in 0.1 M phosphate buffer (pH 3-9) was electrolyzed at 1.0 V vs SSCE at 5 °C for ~45 min or until the current passed was that of the background. The solution was diluted to the required concentration before use.

Procedure 2. A slight excess (1.2-fold) of concentrated NaOCl (0.5 M) was added to a solution containing $[(bpy)_2(OH)RuORu(OH)(bpy)_2](ClO_4)_3$ in 0.1 M phosphate buffer (pH = 3-8). The reaction was monitored by visible spectroscopy. Reactions typically took 10 min to go to completion.

Solutions Containing $[(bpy)_2(py)Ru^{III}ORu^{V}(O)(bpy)_2](ClO_4)_4$. To a solution of known concentration of $[(bpy)_2(py)RuORu(OH)(bpy)_2](ClO_4)_4$ was added 0.6 molar equiv of NaOCl in a 0.1 M phosphate buffer (pH = 7). The oxidation to give a red solution was complete within 10 min.[7]

Measurements. Routine UV-vis spectra were recorded on a Hewlett-Packard Model 8450A diode-array spectrophotometer. Spectroelectrochemical experiments were carried out under argon by using an all-quartz three-compartment cell with quartz frits. Near-infrared spectra were recorded on a Cary 17i spectrophotometer. Stopped-flow

(1) (a) Moyer, B. A.; Meyer, T. J. *J. Am. Chem. Soc.* **1978**, *100*, 3601. (b) Moyer, B. A.; Meyer, T. J. *Inorg. Chem.* **1981**, *20*, 436. (c) McHatton, R. C.; Anson, F. C. *Inorg. Chem.* **1984**, *13*, 3936. (d) Diamantis, A. A.; Murphy, W. R., Jr.; Meyer, T. J. *Inorg. Chem.* **1984**, *23*, 3230. (e) Takeuchi, K. J.; Thompson, M. S.; Pipes, D. W.; Meyer, T. J. *Inorg. Chem.* **1984**, *23*, 1845.
(2) (a) Takeuchi, K. J.; Samuels, G. J.; Gersten, S. W.; Gilbert, J. A.; Meyer, T. J. *Inorg. Chem.* **1983**, *22*, 1407. (b) Che, W.-H.; Wong, K.-Y.; Leung, W.-H.; Poon, C.-K. *Inorg. Chem.* **1986**, *25*, 345. (c) Dobson, J. C.; Meyer, T. J. *Inorg. Chem.* **1988**, *27*, 3283.
(3) (a) Gersten, S. W.; Samuels, G. J.; Meyer, T. J. *J. Am. Chem. Soc.* **1982**, *104*, 4029. (b) Gilbert, J. A.; Eggleston, D. S.; Murphy, W. R., Jr.; Geselowitz, D. A.; Gersten, S. W.; Hodgson, D. J.; Meyer, T. J. *J. Am. Chem. Soc.* **1985**, *107*, 3855. (c) Meyer, T. J. In *Oxygen Complexes and Oxygen Activation by Transition Metals*; Martell, A. E., Sawyer, D. T., Eds.; Plenum Press: New York, 1988; p 33.
(4) Rotzinger, F. P.; Muravalli, S.; Comke, P.; Hurst, J. K.; Gratzel, M.; Pern, F.; Frank, A. J. *J. Am. Chem. Soc.* **1987**, *109*, 6619.
(5) (a) Gilbert, J. A.; Geselowitz, D. A.; Meyer, T. J. *J. Am. Chem. Soc.* **1986**, *108*, 1493. (b) Geselowitz, D. A.; Kutner, W.; Meyer, T. J. *Inorg. Chem.* **1986**, *25*, 2015. (c) Dobson, J. C.; Takeuchi, K. J.; Pipes, D. W.; Geselowitz, D. A.; Meyer, T. J. *Inorg. Chem.* **1986**, *25*, 2357.
(6) (a) Che, C.-M.; Wong, K.-Y.; Mak, T. C. W. *J. Chem. Soc., Chem. Commun.* **1985**, 546. (b) Yukawa, J.; Aoyagi, K.; Kurihara, M.; Shirai, K.; Shimizer, K.; Mukaida, M.; Takeuchi, T.; Kakihara, H. *Chem. Lett.* **1985**, 283. (c) Che, C.-M.; Cheng, W.-K. *J. Chem. Soc., Chem. Commun.* **1986**, 1519. (d) Che, C.-M.; Yang, V. W.-W. *J. Am. Chem. Soc.* **1987**, *109*, 1262. (e) Marmion, M. E.; Takeuchi, K. J. *J. Am. Chem. Soc.* **1986**, *108*, 510.
(7) Doppelt, P.; Meyer, T. J. *Inorg. Chem.* **1987**, *26*, 2027.
(8) Vining, W. J.; Meyer, T. J. *Inorg. Chem.* **1986**, *25*, 2023.

0020-1669/88/1327-4478$01.50/0

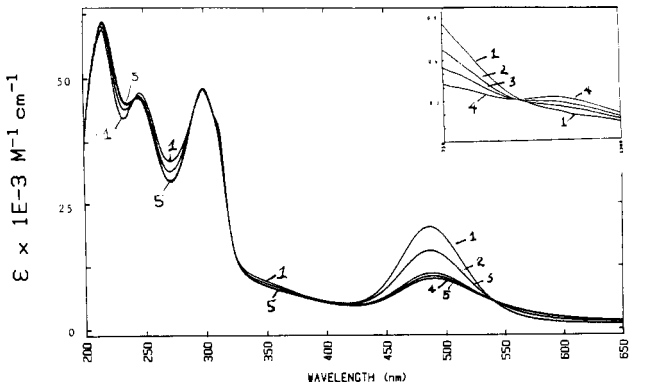

Figure 1. Successive spectral scans during the electrochemical oxidation of $[(bpy)_2(OH)Ru^{III}ORu^{IV}(OH)(bpy)_2]^{3+}$ to $[(bpy)_2(O)Ru^{IV}ORu^{V}(O)(bpy)_2]^{3+}$ at pH = 6 in 0.1 M phosphate buffer at 5 °C. E_{app} = 1.0 V vs SSCE. The insert shows the spectral changes that occur in the near-infrared region.

experiments were performed on a Hi Tech SF-51 stopped-flow apparatus combined with a Zenith 158 microcomputer using an On Line Instrument System (OLIS) stopped-flow program for data acquisition and analysis.

Electrochemical measurements were made by using a PAR Model 173 potentiostat and a PAR Model 175 universal programmer as a sweep generator. Measurements were made by using a platinum-wire auxiliary electrode and a saturated sodium chloride calomel electrode (SSCE) at 25 °C as the reference electrode and are uncorrected for junction potential effects. Electrolyses and coulometry were performed in a three-compartment cell in which the working electrode was a coarse (12 holes/in.) reticulated vitreous carbon electrode (ERG Inc.) connected to a copper wire by using conductive carbon paint (SPI supplies). Measurements of dioxygen in the gas phase were carried out by using a Hewlett-Packard Model 5890 gas chromatography equipped with a 5-Å molecular sieve column (Alltech Assoc.). The column temperature was 90 °C, and the helium gas flow rate was 30 mL/min. A calibration curve was constructed by the injection of known volumes of air samples. Twenty-microliter samples were syringed from the two-compartment airtight cell, and the quantities of O_2 obtained were calculated based on the known 6-mL-volume dead space above the cell. No attempt was made to include the amount of O_2 dissolved in solution. ^1H NMR measurements were performed on a Varian VXR400 400-MHz spectrometer.

Kinetic Measurements. Rate data were obtained by monitoring absorbance changes at 490 nm in either a 1- or 0.1-cm cell depending on the concentration of complex. All measurements were made in phosphate buffer solutions where μ = 0.1 M. Kinetic studies on the oxidation of organic substrates were performed under pseudo-first-order conditions. The first-order rate constants, k, were calculated from a least-squares fit (uniform weighting) of the data to the relation $\ln (A_\infty/A_t) = -k_t + \ln (A_\infty/A_0)$. A_∞ and A_0 are the final and initial absorbances, respectively. A_t is the absorbance at time t. Data were collected over several half-times. The oxidant $[(bpy)_2(O)Ru^{IV}ORu^{V}(O)(bpy)_2]^{3+}$ was generated either by the chemical or electrochemical methods described above and was used in the concentration range 10^{-3}–10^{-5} M.

Results

Chemical and Electrochemical Generation of Ru(IV)–Ru(V). We have developed both chemical and electrochemical methods for the generation of $[(bpy)_2(O)Ru^{IV}ORu^{V}(O)(bpy)_2]^{3+}$ in solution. The net reaction involves the oxidation of the corresponding III–IV complex

$$[(bpy)_2(HO)Ru^{III}ORu^{IV}(HO)(bpy)_2]^{3+} \rightarrow [(bpy)_2(O)Ru^{IV}ORu^{V}(O)(bpy)_2]^{3+} + 2e^- + 2H^+$$

The spectral changes that occur upon electrochemical oxidation of $[(bpy)_2(HO)Ru^{III}ORu^{IV}(OH)(bpy)_2]^{3+}$ at pH 6 at 5 °C and an applied potential of 1.0 V are shown in Figure 1. Cyclic voltammograms of the initial and oxidized solutions were identical, and coulometry (n = 2.01) showed that a total of two electrons were lost during the electrolysis. Reduction of the oxidized solution at an applied potential of 0.6 V occurs with n = 2 to give back $[(bpy)_2(OH)Ru^{III}ORu^{IV}(OH)(bpy)_2]^{3+}$ quantitatively as shown by spectrophotometric measurements.

An attempt was made to isolate the Ru(IV)–Ru(V) μ-oxo complex by the addition of a solution saturated in $Na(ClO_4)$ to a freshly generated, concentrated solution of the IV–V complex. A red-purple precipitate formed, which was found to be unstable and hygroscopic. The ratio of Ru(III)–Ru(IV) to Ru(IV)–Ru(V) present in the solid sample was estimated to be ~1:4 by dissolving the product in a pH = 6 solution and measuring the absorbance change, at 490 nm, as the Ru(III)–Ru(IV) complex appeared at the expense of Ru(IV)–Ru(V). Attempts to purify the precipitate resulted in further decomposition to the lower oxidation state. As for the mixed-valence complex, the oxidation state label is only descriptive; the strong electronic coupling that exists between the Ru sites probably leads to delocalization and the more appropriate oxidation-state description Ru(IV.5)–Ru(IV.5).

The addition of a near-stoichiometric amount of the two-electron oxidant NaOCl to the III–IV complex gives identical spectral changes, over a time period of 5–15 min.

$$[(bpy)_2(OH)Ru^{III}ORu^{IV}(OH)(bpy)_2]^{3+} + HOCl \rightarrow [(bpy)_2(O)Ru^{IV}ORu^{V}(O)(bpy)_2]^{3+} + Cl^- + \tfrac{1}{2}O_2 + H^+$$

As will be reported in a later manuscript,[9] the III–IV/IV–V couple acts as a facile catalyst for the decomposition of HOCl into O_2 and Cl^- in the presence of excess HOCl.

Solutions containing the monosubstituted pyridine complex $[(bpy)_2(py)Ru^{III}ORu^{V}(O)(bpy)_2]^{3+}$ were generated by the addition of 0.6 equiv of NaOCl to solutions containing $[(bpy)_2(py)Ru^{III}ORu^{IV}(OH)(bpy)_2]^{3+}$. The spectral changes in the visible region coincided with those reported by using Ce(IV) as the oxidant in acidic solution.[7]

Properties of the Ru(IV)–Ru(V) Complex. From the spectral changes shown in Figure 1, the oxidation of Ru(III)–Ru(IV) to Ru(IV)–Ru(V) leads to a decrease in intensity of the absorption feature at λ_{max} = 490 nm with the molar extinction coefficient falling from 22 000 to 9700 M^{-1} cm^{-1}. A distinct broadening of the band on the low-energy side also occurs, resulting in isosbestic behavior at 530 nm. Spectral fitting routines, using Gaussian-shaped absorption profiles, suggest that the lower energy shoulder arises from one or more additional, broad absorption features having $\epsilon^{max} \approx 1000$ M^{-1} cm^{-1}.[10] More subtle changes can be seen in other parts of the spectrum; a shoulder at 310 nm and a band at 350 nm both disappear upon oxidation. In the near-infrared region, a band characteristic of the III–IV complex at 1100 nm disappears as the IV–V oxidation state appears.

The IV–V ion can be generated in the pH region 2.5–10. Above pH = 7 it becomes unstable, increasingly so as the pH is raised, because of oxidative decomposition of the bpy ligand.[11] From the $E^{0\prime}$–pH characteristics of the V–V/IV–V and IV–V/III–IV couples, oxidation state IV–V is predicted to be unstable with respect to disproportionation at pH < 2.5.[3b] This prediction was confirmed by mixing a solution containing the Ru(IV)–Ru(V) ion (10^{-4} M) at pH 4 (0.1 M phosphate buffer) with an equal volume of 1.0 M trifluoromethanesulfonic acid, to give a final pH of 1.3. The spectral changes that occurred were quantitatively consistent with the disproportionation in reaction 1.

Oxidation of Water to Dioxygen. The ability of the IV–V complex to oxidize water to dioxygen was investigated both by a kinetic study and by O_2 analysis. The kinetics of H_2O oxidation were followed as the appearance of the III–IV complex by spectrophotometric monitoring at either 530 or 490 nm at 25 °C. The pH was varied by using 0.1 M phosphate buffer solutions. The appearance of the III–IV complex followed wavelength-independent first-order kinetics via the rate law

$$d[Ru(III)–Ru(IV)]/dt = k_{obs}[Ru(IV)–Ru(V)]$$

In monitoring the kinetics of loss of the IV–V complex, two experimental problems were encountered. (1) The rate of reaction

(9) Raven, S. J.; Meyer, T. J., manuscript in preparation.
(10) Raven, S. J.; Neyhart, G. A., unpublished results.
(11) (a) Roecker, L.; Kutner, W.; Gilbert, J. A.; Simmons, M.; Murray, R. W.; Meyer, T. J. *Inorg. Chem.* **1985**, *24*, 3784. (b) Ghosh, P. K.; Brunschwig, B. S.; Chen, M.; Creutz, C.; Sutin, N. *J. Am. Chem. Soc.* **1984**, *106*, 4772. (c) Nord, G.; Pedersen, B.; Bjergbakkir, E. *J. Am. Chem. Soc.* **1983**, *105*, 1913.

Table I. Rate Constants for the Disappearance of $[(bpy)_2(O)Ru^{IV}ORu^{V}(O)(bpy)_2]^{3+}$ as a Function of pH at 25.0 ± 0.1 °C and μ = 0.1 M

pH[a]	10^4[dimer], M^{-1}	$10^4 k^{obsd}$, s^{-1}	
		electrochemical[b]	chemical[b]
2.5	8.0	2.4	3.1
4.4	2.5	2.5	3.0
6.0	8.0	3.3	3.6
	8.0	3.3	
8.5	8.0	5.9	5.8
10.8	8.0	1.7	

[a] In 0.1 M H_2NaPO_4/HNa_2PO_4 buffer. [b] The IV–V complex was generated by electrolysis or by oxidation by HOCl.

Table II. Rates of Oxidation of Organic Substrates by the μ-Oxo Oxidants at 25.0 ± 0.5 °C and μ = 0.1 M in H_2O

substrate	k, M^{-1} s^{-1}		
	μ-oxo complex		monomer
	$(O)Ru^{IV}O-Ru^{V}(O)$[a]	$(py)Ru^{III}O-Ru^{V}(O)$[b]	$[Ru^{IV}(O)-(bpy)_2(py)]^{2+}$[c]
CH_3OH	0.11		3.5×10^{-4}
CH_3CH_2OH	2.4		6.2×10^{-3}
$(CH_3)_2CH(OH)$	2.5	6.9	8.7×10^{-3}
$C_6H_5CH_2OH$	>170		2.3
$(CH_3)_3COH$	0.005		[e]
CH_3CHO	43		0.67
$(CH_3)_2CO$	0.017		
$CH_3CH{=}CHCO_2^-$	50		1.2[d]
$CH_2{=}CH(CH_2)_2CO_2^-$	50	170	1.2[d]

[a] $[(bpy)_2(O)Ru^{IV}ORu^{V}(O)(bpy)_2]^{3+}$ at pH = 5.8 (0.1 M phosphate buffer). [b] $[(bpy)_2(py)Ru^{III}ORu(O)(bpy)_2]^{4+}$ at pH = 5.8. [c] Reference 17. [d] Reference 18. [e] No apparent reaction.

was very susceptible to even trace organic impurities. Special care was required to ensure that all reagents and solvents were uncontaminated. The most reproducible results were obtained if the IV–V complex was generated by the electrochemical method, in part, because during the electrolysis the dimer acts as its own electrocatalyst to oxidize organic impurities. The later explanation is supported by the small excess of current (5–10%) past the expected n value that was often required to achieve total oxidation. (2) With the generation of oxygen, small bubbles formed on the sides of the cuvette. Their formation and discharge unavoidably cause aberrations in the absorbance–time curves. The values of k_{obs} cited are averages of at least three measurements and could have errors as large as ±50%.

Within experimental error, the data collected in Table I show that at pH < 7 the rate of water oxidation is independent of $[H^+]$. The increased rate of disappearance of Ru(IV)–Ru(V) as the pH is increased is not from an accelerated rate of water oxidation but rather because of self-oxidation of coordinated bpy in the complex.[11a]

The stoichiometry of the oxidation of water to dioxygen by the IV–V complex was investigated by gas chromatography. A solution of $[(bpy)_2(HO)Ru^{III}ORu^{IV}(HO)(bpy)_2]^{3+}$ at pH 5.5 was mixed with a stoichiometric amount of NaOCl in a closed, degassed vessel. Samples of the gas in the dead space above the solution were taken 5 h later and compared with a calibration curve of peak height vs volume of O_2 injected. An average of 95% of the oxygen expected based on the number of moles of Ru(IV)–Ru(V) initially present was obtained, thus verifying the stoichiometry

$$2[(bpy)_2(O)Ru^{IV}ORu^{V}(O)(bpy)_2]^{3+} + 2H_2O \rightarrow 2[(bpy)_2(HO)Ru^{III}ORu^{IV}(OH)(bpy)_2]^{3+} + O_2 \quad (2)$$

The stoichiometry of the oxidation by HOCl must be carefully controlled since Ru(IV)–Ru(V) does oxidize HOCl to O_2.[9]

Oxidation of Organic Substrates. Kinetics. The ability of the IV–V complex to act as an oxidant toward a variety of organic substrates was investigated by a series of kinetic studies, the results of which are summarized in Table II. The disappearance of the IV–V complex was followed by observing the change in absorbance at 490 nm. In all cases, at pH 5.8 (μ = 0.1 M) at 25 °C, the experimental rate laws were found to be

$$-d[Ru(IV)-Ru(V)]/dt = k[substrate][Ru(IV)-Ru(V)] = k_{obs}[Ru(IV)-Ru(V)]$$

The net reactions involve the production of the III–IV complex, in net 2e steps, e.g.

$$[(bpy)_2(O)Ru^{IV}ORu^{V}(O)(bpy)_2]^{3+} + CH_3CHOHCH_3 \rightarrow [(bpy)_2(OH)Ru^{III}ORu^{IV}(OH)(bpy)_2]^{3+} + CH_3COCH_3 \quad (3)$$

For some of the more reactive substrates, further reduction of $[(bpy)_2(HO)Ru^{III}ORu^{IV}(HO)(bpy)_2]^{3+}$ to $[(bpy)_2(H_2O)Ru^{III}O-Ru^{III}(H_2O)(bpy)_2]^{4+}$ occurred but the two reaction rates were sufficiently separated timewise that the initial oxidation could be studied separately. However, for some cases overlap between the reactions at long times necessitated the adjustment of the final absorbance (A_∞) for the first reaction in order to obtain satisfactory correlation coefficients in the kinetic fits.

In the presence of large excesses of the organic substrate, k_{obs} was found to be linearly dependent upon the substrate concentration, as shown in Figure 2. Values of k were derived from plots of k_{obs} vs [substrate] with the substrate concentration being varied over at least a 10-fold range.

With both acetone and *tert*-butyl alcohol (Figure 3) and to a lesser extent propanoic, propenoic, and crotonic acids, plots of k_{obs} vs substrate deviated from linearity with k_{obs}, with the effect increasing at lower substrate concentrations. This behavior is expected for cases where the product of the initial oxidation has a considerably higher intrinsic reactivity toward Ru(IV)–Ru(V) than does the initial substrate.

Kinetic studies based on the related pyridine complex $[(bpy)_2(py)Ru^{III}ORu^{V}(O)(bpy)_2]^{4+}$ were complicated by the presence of a small fraction of a slow component. The reactions are sufficiently well separated that it was possible to make rea-

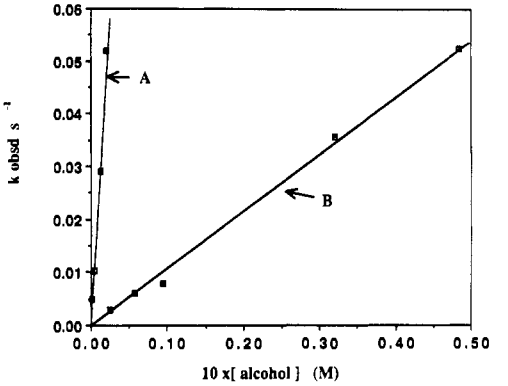

Figure 2. Plot of k_{obs} vs (A) $[(CH_3)_2CHOH]$ and (B) $[CH_3OH]$ at 25 °C in pH = 6 phosphate buffer (μ = 0.1 M) for oxidation by $[(bpy)_2(O)Ru^{IV}ORu^{V}(O)(bpy)_2]^{3+}$.

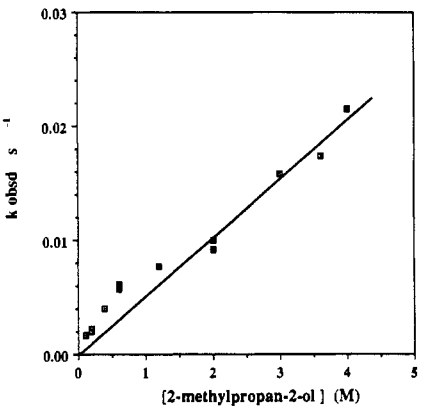

Figure 3. Plot of k_{obs} vs $[(CH_3)_3COH]$ at 25 °C in pH = 6 phosphate buffer for oxidation by $[(bpy)_2(O)Ru^{IV}ORu^{V}(O)(bpy)_2]^{3+}$.

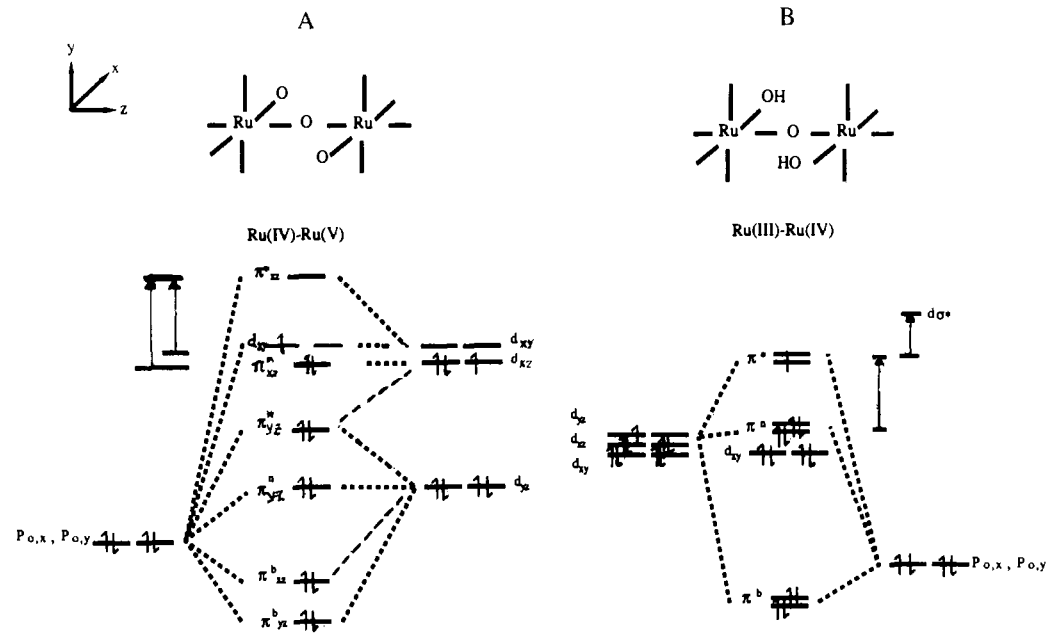

Figure 4. Schematic energy-level diagrams for the complexes $[(bpy)_2(O)Ru^{IV}ORu^{V}(O)(bpy)_2]^{3+}$ (A) and $[(bpy)_2(OH)Ru^{III}ORu^{IV}(OH)(bpy)_2]^{3+}$ (B). Proposed spectral assignments are indicated by the vertical arrows.

sonable estimates of the A_∞ value appropriate for the more rapid component.

Rate laws involving the pyridyl complex were also first order in substrate and first order in complex. Under the conditions of the kinetics experiments, the product is the III–IV complex. A typical net reaction is

$$2[(bpy)_2(py)Ru^{III}ORu^{V}(O)(bpy)_2]^{4+} + (CH_3)_2CHOH \rightarrow 2[(bpy)_2(py)Ru^{III}ORu^{IV}(OH)(bpy)_2]^{4+} + (CH_3)_2CO \quad (4)$$

The 1e character of the final product of reaction has no mechanistic implications. Even if the initial redox step involved a 2e change to give III–III, in the presence of V–V, comproportionation to give the III–IV complex would occur

$$[(bpy)_2(py)Ru^{III}ORu^{V}(O)(bpy)_2]^{4+} + [(bpy)_2(py)Ru^{III}ORu^{III}(OH_2)(bpy)_2]^{4+} \rightarrow 2[(bpy)_2(py)Ru^{III}ORu^{IV}(OH)(bpy)_2]^{4+} \quad (5)$$

Because of the stoichiometry of reaction 3 by which 2 equiv of the oxidant are consumed/equiv of substrate, the experimental rate constants, k_{obs}, are reported in Table II as $k_{obs}/2$ in order to make comparisons with other oxidants.

Discussion

The electrochemical experiments show that the 2e oxidation of $[(bpy)_2(HO)Ru^{III}ORu^{IV}(OH)(bpy)_2]^{3+}$ at pH = 6 leads quantitatively to $[(bpy)_2(O)Ru^{IV}ORu^{V}(O)(bpy)_2]^{3+}$. We have been unable to isolate pure, stable salts of the IV–V complex; the proton composition was inferred in an earlier pH-dependent electrochemical study.[3b] Although resonance Raman spectra have been obtained for the III–III and III–IV complexes,[4,12] we have been unable to observe resonance Raman enhancement for the IV–V complex.

The spectral changes that accompany the III–IV to IV–V conversion include loss of the $\pi \rightarrow \pi^*$(bpy)-based transition at 312 nm characteristic of Ru(III), a decrease in intensity of the band at 498 nm from ϵ = 22000 to ϵ = 9700 M^{-1} cm^{-1}, the appearance of an additional spectral component or components at lower energy, and the loss of a weak band at λ_{max} = 1100 nm.

A schematic molecular orbital diagram first presented by Dunitz and Orgel for the $Ru^{IV}(d^4)$–$Ru^{IV}(d^4)$ ion $[Cl_5RuORuCl_5]^{4-}$[13] has been applied to the III–III complex $[(bpy)_2ClRu^{III}ORu^{III}Cl(bpy)]^{2+}$[14,15] and is reproduced in Figure 4 for the analogous III–IV hydroxo complex. An energy-level diagram is also developed for the IV–V complex in Figure 4. It is assumed that the Ru–O–Ru link is linear in both cases given the absence of the stereochemically important electron pair in the π^* bridging orbitals[16] and the linear Ru–O–Ru link in $[Cl_5RuORuCl_5]^{4-}$.[13] It is also assumed that the oxo groups are trans in the IV–V complex, although the same result would be obtained for a cis arrangement. The axis system used in the diagram has the z axis along the Ru–O–Ru bond. For the IV–V complex, the initial d_π orbital pattern before construction of the Ru–O–Ru interaction includes Ru=O oxo formation at the two metal ions. The basis for oxo formation lies in the mixing of d_{xy} and d_{xz} with the p_x and p_y orbitals of the individual O atoms of the oxo group. Oxo formation imparts antibonding character to d_{xy} and d_{xz} and the ordering $d_{yz} < d_{xy}$,d_{xz} shown in Figure 4A. Compared to Figure 4B, the effect of oxo formation is predicted to lead to a considerable splitting in the d_π orbitals, which after Ru–O–Ru mixing leads to the complex pattern of levels shown.

Although there are a number of possible orbital orderings for the IV–V complex, the one shown having π^*_{yz} lower than π^n_{xz} is consistent with the spectral properties of the complex. Earlier spectral assignments for $[(NH_3)_5RuORu(NH_3)_5]^{5+}$,[15] and by inference for $[(bpy)_2(OH)Ru^{III}ORu^{IV}(OH)(bpy)_2]^{3+}$ as well, assign the low-energy, low-intensity band at 616 nm (at 1100 nm for $[(bpy)_2(OH)Ru^{III}ORu^{IV}(OH)(bpy)_2]^{3+}$) to the transition $\pi^* \rightarrow d\sigma^*$. The M–L σ antibonding levels, $d\sigma^*$, arise from $d_{x^2-y^2}$, d_{z^2} mixing with the σ orbitals of the surrounding ligands. An intense band appears at 342 nm (at 498 nm for $[(bpy)_2(OH)Ru^{III}ORu^{IV}(OH)(bpy)_2]^{3+}$), which has been assigned to the transition to $\pi^n \rightarrow \pi^*$. The intensity of the transition arises from its partial charge-transfer character. A low-intensity band at 255 nm (ϵ = 2100 M^{-1} cm^{-1}) for $[(NH_3)_5RuORu(NH_3)_5]^{5+}$ (at 350 nm for $[(bpy)_2(OH)Ru^{III}ORu^{IV}(OH)(bpy)_2]^{3+}$) has been assigned to the transition $\pi^b \rightarrow \pi^*$. It is not illustrated in Figure 4B.

Turning to $[(bpy)_2(O)Ru^{IV}ORu^{V}(O)(bpy)_2]^{3+}$, we note that the absence of a near-infrared band assignable to the $\pi^* \rightarrow d\sigma^*$ transition is consistent with the empty π^* orbitals. The pattern of orbitals shown in Figure 4A is consistent with the assignment

(12) Raven, S. J.; Kessler, B.; Meyer, T. J., unpublished results.
(13) Dunitz, J. D.; Orgel, L. E. *J. Am. Chem. Soc.* **1953**, *75*, 2594.
(14) Weaver, T. R.; Meyer, T. J.; Adeyemi, S. A.; Brown, G. M.; Eckberg, R. P.; Hatfield, W. E.; Johnson, E. C.; Murray, R. W.; Untereker, D. *J. Am. Chem. Soc.* **1975**, *97*, 3039.
(15) Burchfield, D. E.; Richman, R. M. *Inorg. Chem.* **1985**, *24*, 882.
(16) Llobet, A.; Meyer, T. J., submitted for publication.

$\pi^n_{xz} \rightarrow \pi^*_{xz}$ for the visible band at 498 nm. The decrease in intensity compared to the III–IV complex is, in part, explained by there being two nearly degenerate $\pi \rightarrow \pi^*$ transitions for the latter. According to the diagram, the lower intensity band that appears in the region 550 to 750 nm can be assigned to the transition $d_{xy} \rightarrow \pi^*_{xz}$.

Even though the intense visible absorption bands for the III–IV and IV–V complexes may have the same $\pi^n \rightarrow \pi^*$ origin, the fact that their energies nearly coincide is accidental. The Ru=O interaction probably plays an important role in bringing the $\pi^n \rightarrow \pi^*$ transition for the IV–V complex into the visible. The Ru=O interaction imparts considerable antibonding character to d_{xy} and d_{xz}, which decreases the gap between them and the π^*_{xz} acceptor level.

Solution Chemistry. The Ru(IV)–Ru(V) complex does act as a stoichiometric oxidant for the oxidation of H_2O to O_2 as shown by the oxygen analysis results. The pathway involved is first order in Ru(IV)–Ru(V) and appears to be similar to that found for the monosubstituted pyridine complex $[(bpy)_2(py)Ru^{III}ORu^{V}(O)(bpy)_2]^{4+}$.[7] In the latter case there is a potential ambiguity since the loss of pyridine could lead to the Ru(IV)–Ru(V) complex, which could conceivably account for the results. In the case of the Ru(IV)–Ru(V) complex, if the mechanism of oxidation involved the Ru(V)–Ru(V) complex, it would have to occur via an initial disproportionation

$$2\text{Ru(IV)–Ru(V)} \rightarrow \text{Ru(V)–Ru(V)} + \text{Ru(IV)–Ru(IV)}$$

It would be followed by a second disproportionation

$$2\text{Ru(IV)–Ru(IV)} \rightarrow \text{Ru(IV)–Ru(V)} + \text{Ru(III)–Ru(IV)}$$

since the intermediate oxidation state Ru(IV)–Ru(IV) is unstable with respect to disproportionation.[3b]

The net reaction to give V–V

$$2H^+ + 3[(bpy)_2(O)Ru^{IV}ORu^{V}(O)(bpy)_2]^{3+} \rightarrow 2[(bpy)_2(O)Ru^{V}ORu^{V}(O)(bpy)_2]^{4+} + [(bpy)_2(HO)Ru^{III}ORu^{IV}(HO)(bpy)_2]^{3+}$$

is nonspontaneous at pH > 2, e.g., $\Delta G^{\circ\prime} = +0.64$ eV at pH = 7 and, in any case, is inconsistent with the simple first-order kinetics observed for water oxidation. Thus it appears that an intrinsic water oxidation pathway exists for the IV–V complex based on its ability as a 2e oxidant with k(25 °C, μ = 0.1 M) = 3×10^{-4} s^{-1}.

This is an important observation since it demonstrates that a less than 4e equivalent oxidant does oxidize H_2O to O_2 in a kinetically well-defined pathway. Closely related pathways may also exist, for example, for simple monomeric complexes if they are sufficiently strong as oxidants to carry out the reaction.

The oxidation of water by the IV–V complex at pH = 2.5–7 is slower than by the V–V complex at pH = 1 by a factor of ~100. For Ru(IV)–Ru(V) as a 2e oxidant, water oxidation is thermodynamically spontaneous, reaction 2 with $\Delta G^{\circ\prime} = -1.1$ eV at pH = 7, but requires 2 equiv of oxidant. Initial steps involving the transfer of 2 or 3 oxidative equiv and the formation of H_2O_2 or HO_2 are thermodynamically unfavorable

$$[(bpy)_2(O)Ru^{IV}ORu^{V}(O)(bpy)_2]^{3+} + 2H_2O \rightarrow [(bpy)_2(OH)Ru^{III}ORu^{IV}(OH)(bpy)_2]^{3+} + H_2O_2$$

$$\Delta G^{\circ\prime} = +0.56 \text{ eV}$$

$$[(bpy)_2(O)Ru^{IV}ORu^{V}(O)(bpy)_2]^{3+} + 2H_2O \rightarrow [(bpy)_2(OH)Ru^{III}ORu^{III}(OH_2)(bpy)_2]^{3+} + HO_2$$

$$\Delta G^{\circ\prime} = +1.02 \text{ eV}$$

For the V–V complex there is an intramolecular 4e capability for water oxidation via the V–V/III–III couple:

$$[(bpy)_2(O)Ru^{V}ORu^{V}(O)(bpy)_2]^{4+} + 2H_2O \rightarrow [(bpy)_2(H_2O)Ru^{III}ORu^{III}(H_2O)(bpy)_2]^{4+} + O_2$$

$$\Delta G^{\circ\prime} = -0.72 \text{ eV}$$

Without further insight, the mechanistic details of water oxidation remain obscure. Initial redox steps involving intermediate peroxo formation, e.g.

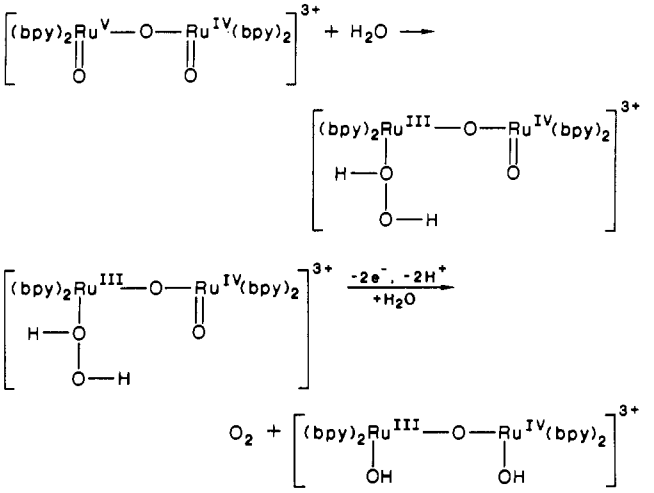

could play an important role, but such intermediates remain to be detected.

The instability of the IV–V complex toward oxidation of bpy in basic solutions has already been mentioned. In acidic solution, as predicted by the pH dependences of the couples,[3b] the complex is unstable with respect to disproportionation (reaction 1).

At initial concentrations of the IV–V complex of $>1 \times 10^{-4}$ M, the disproportionation reaction is rapid ($t_{1/2} < 10$ ms) at pH < 2.5 as shown by a stopped-flow experiment. The rapid disproportionation reaction provides an experimental basis for generating the V–V complex and for following the subsequent water oxidation step. Rapid mixing experiments show that the Ru(V)–Ru(V) μ-oxo ion also absorbs in the region 400–650 nm with a higher molar extinction coefficient than the IV–V complex. From kinetic studies on the disappearance of the V–V complex generated by disproportionation, the rate of water oxidation is a first-order process

$$-\text{d[Ru(V)–Ru(V)]}/dt = k_{obs}[\text{Ru(V)–Ru(V)}]$$

with k(25 °C, μ = 0.1) = 1×10^{-2} s^{-1}.

Organic Oxidation. As can be seen from the data in Table II the enhanced thermodynamic oxidizing strength of the IV–V complex leads to accelerated rates of oxidation of a series of organics when this complex is compared to $[(bpy)_2(py)Ru^{IV}(O)]^{2+}$. The potentials for the appropriate 1e and 2e couples vs SSCE at pH = 7, μ = 0.1 M are as follows:[1b,3a,b,7]

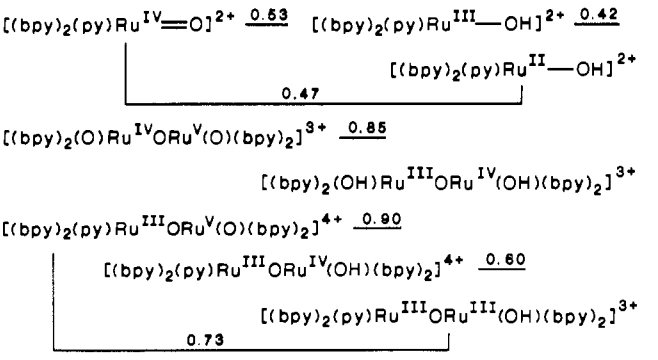

The increased oxidizing strengths for the two μ-oxo oxidants lead to significant rate enhancements (e.g., CH_3OH in Table II) or to oxidations that are otherwise unobservable (e.g., $(CH_3)_3COH$). The extent of rate enhancement between $[(bpy)_2(O)Ru^{IV}ORu^{V}(O)(bpy)_2]^{3+}$ and $[(bpy)_2(py)Ru^{IV}(O)]^{2+}$ is substrate dependent: ~300 for the alcohols ~60 for the aldehyde, ~40 for the olefins.

We have not yet carried out detailed product and mechanistic studies. However, we have shown that the IV–V/III–IV couple

of $[(bpy)_2(O)Ru^{IV}ORu^{V}(O)(bpy)_2]^{3+}$ is an effective electrocatalyst for the oxidation of 2-propanol to acetone. A variety of distinct oxidative mechanistic pathways have been identified for $[(bpy)_2(py)Ru^{IV}(O)]^{2+}$ including examples of O-atom transfer, H-atom transfer, hydride transfer, and ring attack on phenols.[17,19,20] These pathways may also exist for the μ-oxo oxidants, but additional pathways may also appear and the full scope of these reagents remains to be exploited.

Acknowledgment is made to the National Institutes of Health under Grant No. 5-R01-GM32296-05 and to the National Science Foundation under Grant No. CHE-8601604 for support of this research.

(17) (a) Roecker, L.; Meyer, T. J. *J. Am. Chem. Soc.* **1987**, *109*, 746. (b) Meyer, T. J. *J. Electrochem. Soc.* **1984**, *131*, 221C. (d) Thompson, M. S.; Meyer, T. J. *J. Am. Chem. Soc.* **1982**, *104*, 5070.
(18) Raven, S. J.; Meyer, T. J., unpublished results.
(19) (a) Binstead, R. A.; Moyer, B. A.; Samuels, G. J.; Meyer, T. J. *J. Am. Chem. Soc.* **1981**, *103*, 2897. (b) Binstead, R. A.; Meyer, T. J. *J. Am. Chem. Soc.* **1987**, *109*, 3287.
(20) (a) Dobson, J. C.; Seok, W. K.; Meyer, T. J. *Inorg. Chem.* **1986**, *25*, 1614. (b) Roecker, L.; Dobson, J. C.; Vining, W. J.; Meyer, T. J. *Inorg. Chem.* **1987**, *26*, 779. (c) Seok, W. K.; Meyer, T. J. *J. Am. Chem. Soc.*, in press.

Contribution from the Department of Chemistry, University of Alberta, Edmonton, Alberta, Canada T6G 2G2

Kinetics and Products of the Complexation of $(H_2O)_5CrCH_2CN^{2+}$ by Pyrophosphate and Phosphate Ions

M. J. Sisley and R. B. Jordan*

Received April 26, 1988

The kinetics and products of the reactions of phosphate and pyrophosphate ions with $(H_2O)_5CrCH_2CN^{2+}$ have been studied in aqueous acid. In both cases, the reaction proceeds in three discernible stages. The first step on the stopped-flow time scale is assigned to displacement of the water trans to the alkyl ligand with rate constants (M^{-1} s^{-1}, 25 °C, 1.00 M $NaClO_4/HClO_4$) of 0.63 ($H_2P_2O_7^{2-}$), 0.50 ($H_3P_2O_7^-$), 0.47 ($H_2PO_4^-$), and 0.07 (H_3PO_4). The kinetics also yield equilibrium constants for this step of 15 and 3.1 M^{-1} for $H_2P_2O_7^{2-}$ and $H_2PO_4^-$, respectively. The second stage is attributed to isomerization from the trans to the cis position with rate constants of 1.4×10^{-3}, 5.3×10^{-4}, and 1.1×10^{-3} s^{-1} for the $H_2P_2O_7^{2-}$, $H_3P_2O_7^-$, and $H_2PO_4^-$ complexes, respectively. This is followed by a rapid second anation, and finally the bis complex loses its alkyl group with measurable rate constants of 2×10^{-4} and 6×10^{-4} s^{-1} for the pyrophosphate and phosphate systems, respectively. The expected products after the first and last stages have been separated by ion-exchange chromatography and characterized by their electronic spectra. The results are compared to those of previous studies.

Introduction

A number of studies have shown that pentaaquachromium(III) alkyl complexes undergo remarkably rapid reactions with nucleophiles as shown in eq 1. These results have been summarized

$$(H_2O)_5CrCH_2CN^{2+} + X \rightarrow (H_2O)_4(X)CrCH_2CN^{2+} \quad (1)$$

in a recent review.[1] This reactivity has been associated with the trans effect of the alkyl ligand.

In the past 2 years, we have observed that $(H_2O)_5CrCH_2CN^{2+}$ reacts with nucleophiles such as oxalate[2] and hypophosphite[3] to give further substitution coupled with isomerization and chelation in the case of oxalate. The present work was undertaken to explore the reactivity patterns for these processes with phosphate and pyrophosphate as nucleophiles. It is also possible that the results might be relevant to the general coordination chemistry and preparative methods for chromium(III) complexes of phosphate, pyrophosphate, and derivatives such as AMP and ADP.[4,5]

Results

Spectrophotometric Observations and Products with Pyrophosphate. The reaction of $(H_2O)_5CrCH_2CN^{2+}$ with excess pyrophosphate in dilute aqueous acid proceeds in at least three stages, which are discernible from changes in the electronic spectrum. The initial change on the stopped-flow time scale causes a general increase in absorbance with the largest change at ~355 nm. This is followed by a small absorbance increase at the 408-nm peak of the reactant. Within about 10 min, there is a much larger decrease in absorbance at 408 nm with a shift in the maximum to longer wavelength. An isosbestic point is retained at ~485 nm for ~20 min, but this is lost and a new isosbestic point near 605 nm persists after ~1 h until the end of the reaction. During the slower stages, the 525-nm maximum of the reactant disappears and a new peak appears near 625 nm.

The final product solution is apple green, and the electronic spectrum (Table I) corresponds to that of the bis(pyrophosphato)chromium(III) complex reported by DePamphilis and Cleland.[6] This shows that the $-CH_2CN$ ligand has been lost during the overall process. The final product was separated from

Table I. Visible Region Electronic Spectra of Chromium(III) Complexes

complex	wavelength, nm (molar absorptivity, M^{-1} cm^{-1})		sh wavelength, nm	ref
$(H_2O)_5CrCH_2CN^{2+}$	408 (102)	525 (40.1)		*a*
$(H_2O)_5Cr(PO_4H_2)^{2+}$	417 (17.9)	590 (17.3)		*a, b*
$(H_2O)_5Cr(PO_4H_2)^{2+}$	416 (17.2)	591 (16.0)	640, 670	*a, c*
$(H_2O)_5Cr(PO_4H_2)^{2+}$	417 (17.7)	591 (17.1)	640, 670	*a, d*
$(H_2O)_4Cr(PO_4H_2)_2^+$	425 (18.8)	605 (18.3)	640, 675	*a, e*
$(H_2O)_4Cr(PO_4H_2)_2^+$	433 (23.1)	609 (22.4)	644, 678	*a, f*
$(H_2O)_5Cr(P_2O_7H_2)^+$	417 (18.0)	593 (17.1)		*a, g*
$(H_2O)_5Cr(P_2O_7H)$	424 (22.4)	594 (22.7)		*h*
$(H_2O)_5Cr(P_2O_7H)$	425 (25.0)	595 (24.0)		*i*
$(H_2O)_4Cr(P_2O_7H_2)_2^-$	441 (20.8)	624 (20.0)	650, 680	*a, j*
$(H_2O)_4Cr(P_2O_7H_2)_2^-$	441 (21)	626 (20)	650, 680	*k*

[a] This work. [b] The 2+ product after 75 s and treatment with Hg(II). [c] Product from Cr(II) and $(NH_3)_4CoPO_4$. [d] The 2+ product after 102 min and treatment with Hg(II). [e] The <2+ product after 102 min and treatment with Hg(II). [f] Solid dissolved in 0.01 M perchloric acid. [g] The 2+ product after 90 s and treatment with Hg(II), in 0.01 M perchloric acid. [h] As in footnote *g*, except pH 5.5. [i] Reference 9. [j] Final product in ~0.01 M perchloric acid. [k] Reference 6.

(1) Espenson, J. H. *Adv. Inorg. Bioinorg. Mech.* **1982**, *1*, 1.
(2) Sisley, M. J.; Jordan, R. B. *Inorg. Chem.* **1987**, *26*, 273.
(3) Sisley, M. J.; Jordan, R. B. *Inorg. Chem.* **1987**, *26*, 2833.
(4) Cleland, W. W. *Methods Enzymol.* **1982**, *87*, 159.
(5) Lin, I.; Dunaway-Mariano, D. *J. Am. Chem. Soc.* **1988**, *110*, 950 and references therein.
(6) DePamphilis, M. L.; Cleland, W. W. *Biochemistry* **1973**, *12*, 3714.

0020-1669/88/1327-4483$01.50/0